Water Resources Research

RESEARCH ARTICLE
10.1029/2023WR035644

Reconstruction of the Pleistocene Paleoclimate From Deep Groundwater in Southern Germany From Noble Gas Temperatures Linked With Organic Radiocarbon Dating

Theis Winter[1], Werner Aeschbach[2], and Florian Einsiedl[1]

[1]Chair of Hydrogeology, School of Engineering and Design, Technical University of Munich, Munich, Germany, [2]Institute of Environmental Physics, Heidelberg University, Heidelberg, Germany

Key Points:

- The noble gas temperatures from deep groundwater in Southern Germany show substantial cooling up to 8°C during the Pleistocene
- Noble gas temperatures in combination with groundwater dating using the $^{14}C_{DOC}$ method are helpful for reconstructing the paleoclimate
- The deep groundwater in the Upper Jurassic aquifer may be a mixture of meteoric water and Pleistocene glacial meltwater

Supporting Information:

Supporting Information may be found in the online version of this article.

Correspondence to:

F. Einsiedl,
f.einsiedl@tum.de

Citation:

Winter, T., Aeschbach, W., & Einsiedl, F. (2024). Reconstruction of the Pleistocene paleoclimate from deep groundwater in Southern Germany from noble gas temperatures linked with organic radiocarbon dating. *Water Resources Research*, *60*, e2023WR035644. https://doi.org/10.1029/2023WR035644

Received 20 JUL 2023
Accepted 15 DEC 2023

Author Contributions:

Conceptualization: Theis Winter, Florian Einsiedl
Funding acquisition: Florian Einsiedl
Methodology: Theis Winter, Werner Aeschbach
Project Administration: Theis Winter, Florian Einsiedl
Software: Theis Winter, Werner Aeschbach
Supervision: Florian Einsiedl
Validation: Theis Winter, Werner Aeschbach, Florian Einsiedl
Visualization: Theis Winter

Abstract This study presents a 25 ka reconstruction of the Pleistocene paleoclimate in the South German Molasse Basin. Deep groundwater was sampled at 19 wells in the Upper Jurassic aquifer (UJA). Calculating gas temperatures (NGT) using the UA model with the noble gases Ar, Kr, and Xe led to groundwater recharge temperatures between 0.4 and 4.7°C. Combined with innovative $^{14}C_{DOC}$ groundwater dating, calculated NGTs revealed up to 8°C cooler soil temperatures during the Pleistocene compared with modern soil temperature. This interpretation agrees well with the observed depleted stable water isotope signature ranging from −83.3 to −86.1 for δ^2H and from −10.66 to −11.77 for $\delta^{18}O$, which is characteristic of groundwater of Pleistocene origin in Southern Germany. The temperature differences (ΔT) agree remarkably well with calculated NGTs within other European basins (ΔT 6–9.5°C) and suggest widespread pronounced terrestrial cooling during the Last Glacial Maximum through the interior of the European continent.

Plain Language Summary To characterize the climate in Southern Germany during the last ice age, we first determined $^{14}C_{DOC}$ for dating the deep groundwater of the Upper Jurassic aquifer. Subsequently, we looked closer at noble gases and stable water isotopes. The contents in groundwater are mainly controlled by temperature when the groundwater is in contact with the atmosphere during the formation on the earth's surface. Our results show that the calculated noble gas temperatures during this time were up to 8°C colder than modern temperatures. Our findings help to gain a better understanding of Earth's climatic history.

1. Introduction

Understanding the mechanisms of past climate change can help to predict future changes. Confined groundwater systems represent practical paleoclimate archives, and differences between average Holocene (since 11.7 ka) and Last Glacial Maximum (LGM) climate conditions can often be resolved. The LGM occurred between approx. 26.5 and 19 ka (P. U. Clark et al., 2009).

As the signature of the stable water isotopes in precipitation is strongly temperature-dependent (Dansgaard, 1964), earlier studies used the stable water isotope signatures (δ^2H and $\delta^{18}O$) from ice cores (e.g., Jouzel & Masson-Delmotte, 2007) to study the climatic temperature changes during glacial and interglacial periods in the Pleistocene. The stable water isotope signatures can further help interpret the sources of groundwater recharge in a glacial environment (Hayashi et al., 2004; Klump et al., 2008). In combination with the radiocarbon method (^{14}C), the paleoclimate can be reconstructed for the Holocene/Pleistocene boundary. However, the stable water isotope signature of the recharged groundwater can also be affected by several processes in the subsurface, such as evaporation or exchange processes with the rock matrix, as well as by mixing with different groundwater components (I. Clark, 2015). The stable water isotope signature alone can lead to misinterpretation and thus must be used in combination with other climate proxies.

In previous studies, the dissolved atmospheric noble gases archived in groundwater were used as indicators of past climate conditions (Seltzer et al., 2021; Stute et al., 1995; Weyhenmeyer et al., 2000). As the solubility of the noble gases in groundwater is temperature-dependent, the noble gas infiltration temperature (NGT) can be estimated from the noble gas record in groundwater (Cey et al., 2009). The NGT reflects the temperature during groundwater recharge, when the freshly infiltrating groundwater equilibrated with the atmosphere, and provides valuable information as a climate proxy. The inert and conservative behavior of the noble gases makes them an ideal parameter for the characterization of paleoclimate information, as there are no significant sinks or sources

Writing – original draft: Theis Winter, Werner Aeschbach, Florian Einsiedl
Writing – review & editing: Theis Winter, Werner Aeschbach, Florian Einsiedl

to be considered for freshly recharged groundwater on glacial-interglacial timescales (Pepin & Porcelli, 2002; Seltzer et al., 2021).

Reconstructing the European paleoclimate during the Pleistocene and Holocene using aquifer systems as paleoclimate archives is challenging, as parts of Europe were covered with glaciers and permafrost.

To date, the effects of the glacial environment on groundwater recharge and processes remain partially unknown (Utting et al., 2013). Several paleoclimate studies from European aquifers show differing groundwater evolution during this time (McIntosh et al., 2012). Some of the studies from aquifer systems located in Belgium (Blaser et al., 2010), England (Andrews & Lee, 1979), and Switzerland (Beyerle et al., 1998) have shown an interruption in continuous groundwater recharge, which occurred during the Late Pleistocene, while other basins show no or no complete cessation of groundwater recharge between 17 and 25 ka (e.g., Broers et al., 2021; Varsányi et al., 2011).

Nevertheless, where groundwater recharge has occurred, global studies in low-to-mid-latitude land surfaces using the noble gas records from groundwater have shown around 6°C cooler temperatures during the LGM compared to the Holocene (Seltzer et al., 2021). The most significant temperature differences between Pleistocene and Holocene that have been obtained from the noble gas record were found in European aquifers in Belgium (Blaser et al., 2010) and Hungary (Varsányi et al., 2011), with a maximum temperature difference of up to 9.5°C.

The deep sedimentary Upper Jurassic aquifer (UJA) in the South German Molasse Basin (SGMB) is composed of fractured and karstified carbonate rocks. The UJA is a vital water resource for thermal energy use, and several hydrochemical studies were conducted only recently to understand the regional and local flow regime in the central part of the basin (Heidinger et al., 2019; Heine & Einsiedl, 2020; Heine et al., 2021; Winter & Einsiedl, 2022). Past climate conditions leave their signature in the chemical and isotopic composition of groundwater and are best preserved in confined aquifers typically found in extended sedimentary basins. Therefore, the UJA may be one of the most interesting aquifers worldwide to study the effects of a glacial environment on deep groundwater flow and circulation in a geothermal setting.

However, it is essential to understand the local and regional flow regimes on the basin scale to interpret NGT as a proxy for the uniform cooling of Southern Germany during the Pleistocene. In addition, although dating appears to be very common in groundwater, using ^{14}C of dissolved inorganic carbon ($^{14}C_{DIC}$) as a dating tool may show uncertainties, particularly in carbonate aquifers. It was stated in earlier papers (Heidinger et al., 2019) that the $^{14}C_{DIC}$ contents in the UJA are lower than 2 pmC. In a recently published paper by Heine and Einsiedl (2020), the capability of the ^{14}C of dissolved organic carbon ($^{14}C_{DOC}$) method as a powerful groundwater dating tool was shown with the potential also to improve the accuracy of paleoclimate studies worldwide.

As a result, Winter and Einsiedl (2022) were able, by combined use of $^{14}C_{DOC}$ and ^{81}Kr, to show that the deep groundwater of the UJA consists of at least two significantly different apparent water ages: an up to now unknown water component stemming from the Pleistocene/Holocene transition and an old component of up to 300,000 years. The new groundwater dating results with $^{14}C_{DOC}$ open the unique chance to use the UJA for paleoclimate reconstruction and compare the results with former studies from European aquifers. In addition, groundwater circulation depths of more than 5 km can be assumed for the UJA. To the best of our knowledge, such a system may be unique worldwide; up to now, no comparable study has used NGTs from such deep aquifers.

Therefore, in this study, we aim to reconstruct the paleoclimate history during the Pleistocene/Holocene transition for the deep UJA in the SGMB using NGT from the noble gas record (Ne, Ar, Kr, and Xe), stable water isotopes, hydrochemistry, and $^{14}C_{DOC}$ apparent groundwater ages, and we will link our results to existing field investigations and noble gas temperatures. The results provide important support for the notion that pronounced terrestrial cooling during the LGM was likely widespread through the interior of the European continent.

2. Materials and Methods

2.1. Groundwater Sampling in the Study Area

The database for this study consists of 19 wells screened in the UJA. Thirteen of these wells are active, geothermally used wells; three are from a newly constructed geothermal plant; and three are research drillings not in continuous production. The location of the wells in the study area is illustrated in Figure 1. The 16 wells used for the geothermal energy production lie at depths between approximately 2,000 and 5,000 m and show groundwater

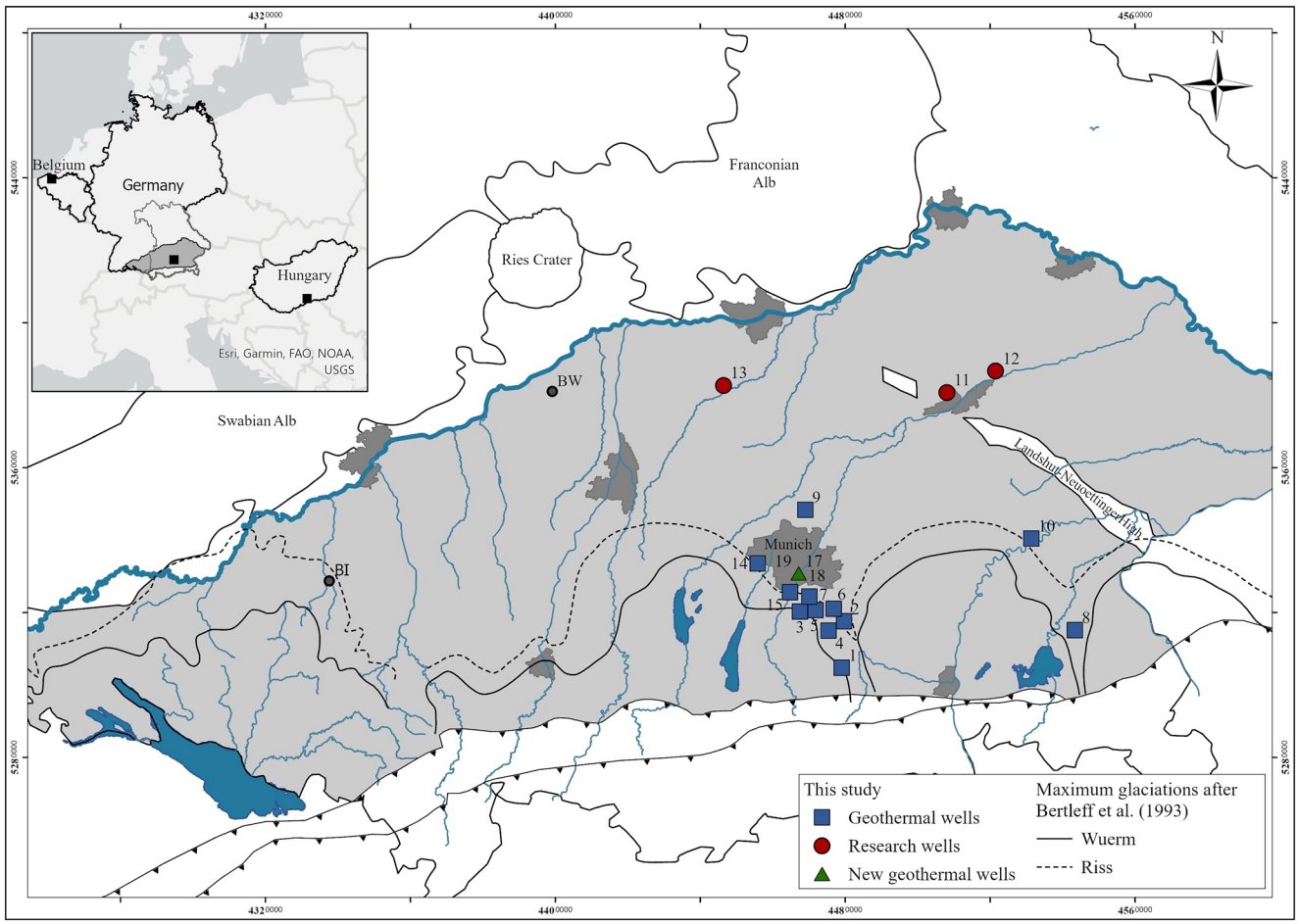

Figure 1. Study area and location of the 19 wells from this study and the two locations BJ and BW in the western part of the South German Molasse Basin (SGMB). The black squares in the inset map in the upper left corner shows the locations of the study are from Blaser et al. (2010) in Belgium, Varsányi et al. (2011) in Hungary and this study in the SGMB. The gray area shows the extent of the SGMB. The figure also shows the maximum extent of the last two major glaciations in the area (Bertleff et al., 1993).

temperatures between 75 and 155°C. The three research wells are in the northern part of the SGMB, at shallower depths between approximately 500 and 800 m, and show lower groundwater temperatures between 20 and 50°C.

All 19 wells were sampled for noble gases, stable water isotopes, and hydrochemistry. In addition, for groundwater samples 1, 2, 3, 4, and 5, $^{14}C_{DOC}$ values from Winter and Einsiedl (2022) were used, while unpublished $^{14}C_{DOC}$ values for samples 11, 12, and 13 were added for data interpretation.

All samples were taken during the regular operation of the geothermal wells. During the sampling, the physicochemical parameters pH, specific electric conductivity (eC), and groundwater temperature (T) were constantly measured with a multi-parameter portable meter (Multi 3430 WTW). The carbonate species HCO^-_3 and H_2CO_3 were determined on-site by titration with 0.1 M HCl and NaOH. The groundwater samples for chemical analysis were field filtered with a 0.22 µm filter. The samples were stored in 50 ml HDPE containers acidified with HNO_3 (65%) for cations and stored at 4°C while the samples for anions were frozen prior to analysis. The major cations and anions were analyzed with an ion chromatograph (Dionex ICS1100 Thermo Fisher Scientific) at the Chair of Hydrogeology at the Technical University of Munich. The analytical error was less than 5%.

The samples for stable water isotopes measurements were taken in 15 ml HDPE vials, which were entirely filled with groundwater—the addition of activated carbon removed hydrocarbons contained in the sample. Before analysis, the sample was filtered with a 0.22 µm filter. Stable water isotope ratios were analyzed with an isotopic water analyzer (IWA-45EP Los Gatos Research) in the Chair of Hydrogeology at the Technical University of Munich. The stable water isotope ratios are expressed in delta notation ($\delta^{18}O$ and δ^2H) relative to the VSMOW standard. The analytical error was <0.1‰ for $\delta^{18}O$ and <1‰ for δ^2H.

For noble gas analysis, groundwater samples were collected in copper tubes mounted in aluminum racks, which were hermetically sealed with stainless steel clamps (Beyerle et al., 2000). Degassing or fractionation processes were minimized by taking uncooled and pressure-controlled samples at operational pressure in the geothermal plants (Nakata et al., 2019). The samples were stored at 4°C until the noble gas isotopes were analyzed using an MM5400 mass spectrometer (Thermo Fisher Scientific) at the Institute of Environmental Physics, Heidelberg University.

For measurement of $^{14}C_{DOC}$ 20 L of groundwater was filled into cleaned HDPE jerry cans, acidified to pH 2 with approximately 25 ml HCl (36%), and stored at 4 ∘C prior to extraction in the laboratory. The extraction of the DOC was done with the SPE-PPL method (Dittmar et al., 2008; Heine & Einsiedl, 2020; Li et al., 2016). The analysis was performed with accelerator mass spectrometry (HVE 3MV Tandetron 4130) at the Leibniz Laboratory for Radiometric Dating and Stable Isotope Research at the Christian-Albrechts University of Kiel.

2.2. Noble Gas Temperature Evaluation Process

The raw noble gas data was fitting and evaluated with the open-source software PANGA (Program for the Analysis of Noble GAs data), following the suggested evaluation process described in Jung and Aeschbach (2018). An updated version of PANGA using the latest noble gas solubilities from Jenkins et al. (2019) was employed. As a first step, fitting of the samples was performed using an inverse modeling approach with the unfractionated excess air (EA) model (UA), as this is the traditional, simplest EA model:

$$C_i(T, S, P, A) = C_i^{eq}(T, S, P) + Az_i \tag{1}$$

T = temperature in °C, S = salinity in g/kg, P = pressure in atm, A = concentration of dissolved EA in ccSTP/g, and z_i = mixing fraction of the specific noble gas in dry air (Jung & Aeschbach, 2018). The UA model assumes the complete dissolution of trapped air in groundwater with the atmospheric composition and is therefore unfractionated (Aeschbach-Hertig et al., 2008; Andrews & Lee, 1979; Stute & Schlosser, 1993). In the UA model, the two parameters, T and A are fitted.

We expect all samples to have the same recharge area, and pressure P is expected to be quite similar for all samples. A P value of 0.948 was used, as suggested by Heine et al. (2021), for the estimation of NGT for the same study area. Salinity S was expected to be 0 at groundwater recharge, as the stable water isotope signatures clearly indicate meteoric origin for samples 1 to 13. He is generally not used for calculation of NGTs as its solubility in water is not very sensitive to temperature, compared to the other noble gases, and the subsurface production of He requires additional corrections (Aeschbach-Hertig & Solomon, 2013).

As suggested by Jung and Aeschbach (2018), for the fitting procedure with the UA model, the following assumptions were taken into account in assessing the noble gas record. Small or very large values of parameter A may indicate an unusual amount of EA, whereas negative values of A indicate degassing. While samples with low χ^2 values and corresponding high fit probabilities meet the requirements and may need no further evaluation steps. It is generally recommended to test more complex EA models, such as the closed-system equilibration (CE) model, which assumes equilibration between groundwater and trapped air bubbles (Aeschbach-Hertig et al., 2000).

$$C_i(T, S, P, A, F) = C_i^{eq}(T, S, P) + \frac{(1 - F) \cdot Az_i}{1 + FAz_i/C_i^{eq}} \tag{2}$$

The parameter F denotes the dimensionless fractionation factor by which the size of the gas phase has changed during re-equilibration. In contrast to the other EA models, the parameter A describes the initial amount of entrapped air per unit mass of water and is measured in cm^3STP/g (Jung & Aeschbach, 2018). Better fits can be expected from models with more free parameters. Still, samples with very high χ^2 values from the UA model often cannot be described by any existing EA model. Overall, the χ^2 fit probabilities should be greater than 1%. Otherwise, the fits are rejected (Aeschbach-Hertig & Solomon, 2013; Aeschbach-Hertig et al., 2000, 2002, 2008).

2.3. Determination of Apparent Groundwater Ages

The apparent $^{14}C_{DOC}$ groundwater ages or piston-flow ages were calculated using 85 pmC as an initial radiocarbon concentration (Geyer et al., 1993), as follows:

$$^{14}t = -8267 \ln \frac{^{14}C_t}{^{14}C_0} \tag{3}$$

Table 1
This Table Contains the Noble Gas Record for the 19 Samples From the Upper Jurassic Aquifer in the South German Molasse Basin Used to Calculate the Noble Gas Temperatures and $^{40}Ar/^{36}Ar$ and $^{20}Ne/^{22}Ne$ Ratios and the Analytical Uncertainties

ID	He	ΔHe	Ne	ΔNe	Ar	ΔAr	Kr	ΔKr	Xe	ΔXe	$^{40}Ar/^{36}Ar$	$^{20}Ne/^{22}Ne$
						[ccSTP/g]						
1	2.46E−05	2.45E−07	2.37E−07	1.35E−09	5.23E−04	2.29E−06	1.21E−07	1.88E−09	1.74E−08	2.40E−10	302.81 ± 4.26	9.80 ± 0.02
2	1.94E−05	1.52E−07	2.25E−07	5.05E−10	4.75E−04	9.70E−07	1.09E−07	1.52E−09	1.62E−08	3.62E−10	294.97 ± 3.98	9.80 ± 0.02
3	4.71E−05	3.55E−07	2.09E−07	4.63E−10	5.01E−04	1.17E−06	1.09E−07	1.64E−09	1.64E−08	2.66E−10	302.05 ± 5.32	9.83 ± 0.02
4	2.42E−05	1.90E−07	2.09E−07	4.70E−10	4.89E−04	9.95E−07	1.11E−07	1.57E−09	1.66E−08	3.57E−10	297.10 ± 4.08	9.81 ± 0.02
5	3.27E−05	2.47E−07	3.19E−07	7.05E−10	5.71E−04	1.33E−06	1.28E−07	2.00E−09	1.93E−08	3.18E−10	300.12 ± 5.16	9.80 ± 0.02
6	2.04E−05	2.55E−07	2.14E−07	1.40E−09	4.76E−04	2.43E−06	1.08E−07	1.31E−09	1.62E−08	2.62E−10	291.60 ± 5.21	9.79 ± 0.04
7	5.16E−05	4.05E−07	1.90E−07	4.28E−10	4.94E−04	9.80E−07	1.10E−07	1.60E−09	1.66E−08	3.60E−10	307.30 ± 4.26	9.81 ± 0.02
8	2.01E−05	2.52E−07	2.31E−07	1.50E−09	4.86E−04	2.51E−06	1.13E−07	1.38E−09	1.59E−08	2.56E−10	291.34 ± 5.08	9.80 ± 0.04
9	2.12E−05	1.82E−07	2.09E−07	1.18E−09	4.76E−04	2.79E−06	1.09E−07	2.03E−09	1.62E−08	2.82E−10	297.94 ± 5.54	9.80 ± 0.04
10	2.17E−05	2.72E−07	2.48E−07	1.61E−09	4.59E−04	2.33E−06	1.07E−07	1.29E−09	1.58E−08	2.46E−10	289.57 ± 5.12	9.78 ± 0.04
11	3.09E−05	2.34E−07	7.40E−07	1.63E−09	5.48E−04	1.28E−06	1.23E−07	1.92E−09	1.75E−08	2.88E−10	296.00 ± 5.36	9.82 ± 0.02
12	2.31E−05	1.81E−07	3.02E−07	6.73E−10	4.79E−04	9.40E−07	1.10E−07	1.61E−09	1.61E−08	3.57E−10	292.64 ± 3.94	9.79 ± 0.02
13	8.53E−07	6.70E−09	2.56E−07	5.74E−10	4.71E−04	9.72E−07	1.09E−07	1.55E−09	1.65E−08	3.80E−10	296.04 ± 4.09	9.79 ± 0.02
14	7.05E−05	5.35E−07	1.89E−08	7.81E−11	7.58E−05	1.87E−07	1.60E−08	3.73E−10	3.65E−09	6.10E−11	352.90 ± 25.79	9.85 ± 0.02
15	8.98E−05	8.69E−07	1.62E−07	9.42E−10	4.54E−04	2.65E−06	6.71E−08	8.09E−09	7.35E−09	3.78E−10	307.80 ± 5.87	9.81 ± 0.04
16	6.89E−05	6.95E−07	3.05E−08	1.79E−10	1.45E−04	6.53E−07	3.62E−08	5.75E−10	6.83E−09	8.76E−11	348.28 ± 5.54	9.93 ± 0.04
17	6.74E−05	9.38E−07	1.58E−07	9.56E−10	3.62E−04	2.04E−06	8.27E−08	9.22E−10	1.27E−08	1.49E−10	306.11 ± 4.90	9.81 ± 0.00
18	7.55E−06	9.05E−08	1.39E−08	8.20E−11	7.02E−05	4.44E−07	2.18E−08	2.30E−10	4.76E−09	5.57E−11	325.36 ± 21.96	10.11 ± 0.02
19	7.52E−06	9.01E−08	1.07E−08	6.34E−11	4.90E−05	3.38E−07	1.53E−08	2.28E−10	3.53E−09	4.70E−11	352.80 ± 26.73	10.11 ± 0.01

where $^{14}C_t$ = measured radiocarbon concentration and $^{14}C_0$ = initial radiocarbon concentration.

Contrary to groundwater dating with dissolved inorganic radiocarbon ($^{14}C_{DIC}$), groundwater dating with dissolved organic radiocarbon ($^{14}C_{DOC}$) has proven to offer the unique possibility to date groundwater in carbonate aquifers, such as the UJA (Heine & Einsiedl, 2020; Winter & Einsiedl, 2022). Advantages to $^{14}C_{DIC}$ are that groundwater dating with $^{14}C_{DOC}$ may not be affected by microbial degradation of organic carbon or masked by isotope dilution processes by biogeochemical processes, the latter one may occur in deep anoxic carbonate aquifers (Geyer et al., 1993; Hershey et al., 2016; Murphy et al., 1989; Thomas et al., 2021).

3. Results and Discussion

3.1. Evaluation of the Noble Gas Record

First, we examined the noble gas concentrations in the groundwater samples to identify any unusual patterns in the data set. As a result, we separated the data set into two groups (Table 1). Examples of group I (samples 1 to 13) showed values between 1.8×10^{-7} and 7.4×10^{-7} ccSTP/g for neon, between 4.5×10^{-4} and 5.7×10^{-4} ccSTP/g for argon, between 1.1×10^{-7} and 1.2×10^{-7} ccSTP/g for krypton and between 1.6×10^{-8} and 1.9×10^{-8} ccSTP/g for xenon. The average analytical error for each noble gas is ±0.4% for Ne and Ar, ±1.4% for Kr, and ±1.7% for Xe.

The noble gas concentrations in group I are in a reasonable range for atmospheric-derived noble gases in groundwater. Samples from group I showed quite a uniform distribution for Ar, Kr, and Xe, while Ne values vary more. Figure 2 shows the measured Xe plotted versus the Ne concentrations, along with the expected lines for air-equilibrated water and the addition of EA. Such a plot is indicative of the main features of the noble gas concentrations, as Xe is most sensitive to temperature. In contrast, Ne is most sensitive to the addition of EA. Ne concentrations above the expected atmospheric solubility equilibrium of about 2.0×10^{-7} ccSTP/g

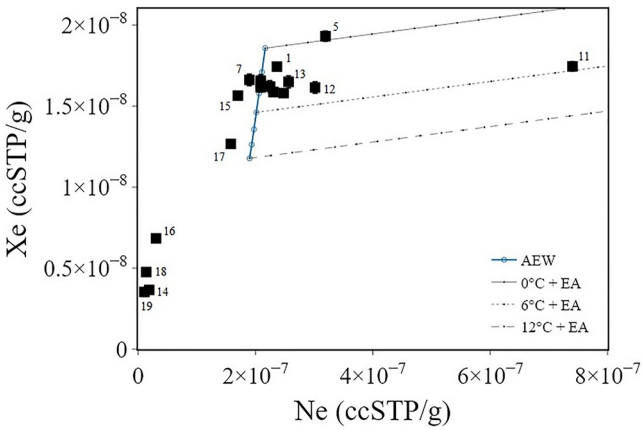

Figure 2. Measured Xe and Ne plot for samples from group I and group II (squares) compared to air-equilibrated water concentrations for 0–12°C and addition of unfractionated excess air.

indicate the presence of EA, while lower Ne concentrations are a hint for degassing effects (Jung & Aeschbach, 2018). Ne concentrations of samples from group I lie close or somewhat above the equilibrium values, except for sample 11, which has the highest Ne concentration, indicating a very large EA component.

In contrast, samples from group II (samples 14 to 19) showed lower noble gas concentrations overall than those from group I. The noble gas concentrations in group II, especially for the lighter noble gases Ne and Ar, deviate significantly from calculated equilibration concentrations for atmospheric-derived noble gases in groundwater. The Ne concentrations in this group lie consistently below the expected equilibrium. Samples 14, 16, 18, and 19 are an order of magnitude lower, clearly indicating the presence of strong degassing. Xe concentrations are also clearly depleted, although somewhat less than Ne concentration (Figure 2).

To exclude the possibility that the Ne and Ar concentrations are affected by a terrigenic or mantle component, we compared the $^{20}Ne/^{22}Ne$ and $^{40}Ar/^{36}Ar$ ratios in our samples (Figure 3d). Considering the analytical error of the measurements, samples of group I are in the range of the atmospheric $^{20}Ne/^{22}Ne$ and $^{40}Ar/^{36}Ar$ ratios (9.80 (Porcelli et al., 2002) and 298.56 (Lee et al., 2006), respectively). Only sample 7 showed an elevated $^{40}Ar/^{36}Ar$ ratio of up to 307.3 ± 4.3, which is marginally significant on the 2σ-level. However, this result does not warrant a correction of the Ar concentration for the possible terrigenic proportion of ^{40}Ar of about 3%. In contrast, the samples from group II showed elevated $^{20}Ne/^{22}Ne$ and $^{40}Ar/^{36}Ar$ ratios above the atmospheric ratios. Only samples 15 and 17, based on their Ne concentrations, are less degassed than the other samples from this group, showed $^{20}Ne/^{22}Ne$ ratios around 9.81 and only slightly elevated $^{40}Ar/^{36}Ar$ ratios like sample 7. The four samples with the lowest gas concentrations (14, 16, 18, and 19) exhibit elevated $^{20}Ne/^{22}Ne$ and also $^{40}Ar/^{36}Ar$ ratios, although measurement uncertainty for ^{36}Ar was high in these samples due to the low gas content. The deviating isotope ratios in the samples from group II could indicate an influence of an older fossil groundwater component, shifting both ratios to the observed elevated values. It should be noted, however, that isotope fractionation due to degassing controlled by diffusion cannot explain both elevated ratios. Such degassing is expected to lead to preferential loss of the lighter, more diffusive isotope. Thus, the elevated $^{40}Ar/^{36}Ar$ ratios could be due to fractionation, but this explanation would be inconsistent with the observed elevated $^{20}Ne/^{22}Ne$ ratios, which should be lowered by diffusive fractionation.

The difference in the noble gas concentrations and $^{20}Ne/^{22}Ne$ and $^{40}Ar/^{36}Ar$ ratios between the samples from group I and group II is likely explained by the groundwater development. A detailed description about the different hydrochemical composition for samples from group I and group II is given in Supporting Information S1. Samples from group I are characterized by an overall low mineralization with TDS between 400 and 780 mg/l and stable water isotopes ranging between −83.3 and −86.1‰ for δ^2H and −10.7 and −11.8‰ for $\delta^{18}O$. In contrast, samples 14 to 19 showed high mineralization with TDS up to 5,100 mg/l and stable water isotopes ranging between −62.2 and −81.6‰ for δ^2H and −3.3 and −10.4‰ for $\delta^{18}O$. Previous studies found clear evidence of an interaction between old, Paleogene, or Neogene formation water, oil formation waters, and the UJA groundwater for these groundwater samples (Heine et al., 2021; Stichler, 1997). It is stated in the literature that pristine oil is free of atmospheric-derived noble gases and acquires them through interaction with reservoir water (Karolytė et al., 2021). Compared to atmospheric-derived groundwater, oil-field waters in the reservoir usually show a depletion in noble gases and may act as a sink for noble gases (Karolytė et al., 2021).

Therefore, the observed low noble gas concentrations and elevated $^{20}Ne/^{22}Ne$ and $^{40}Ar/^{36}Ar$ ratios for samples 14 to 19 in group II may be caused by mixing processes of different groundwater types during the development of this groundwater. However, we can also not exclude degassing effects during the sampling procedure of group II, although sampling was performed quite carefully. Furthermore, attempts to fit the noble gas concentrations of group II wells using existing degassing models as described by Aeschbach-Hertig et al. (2008), such as the CE model with a fractionation parameter $F > 0$ or diffusive degassing models, did not yield satisfactory results. We decided to exclude group II's data set from further consideration for the abovementioned reasons.

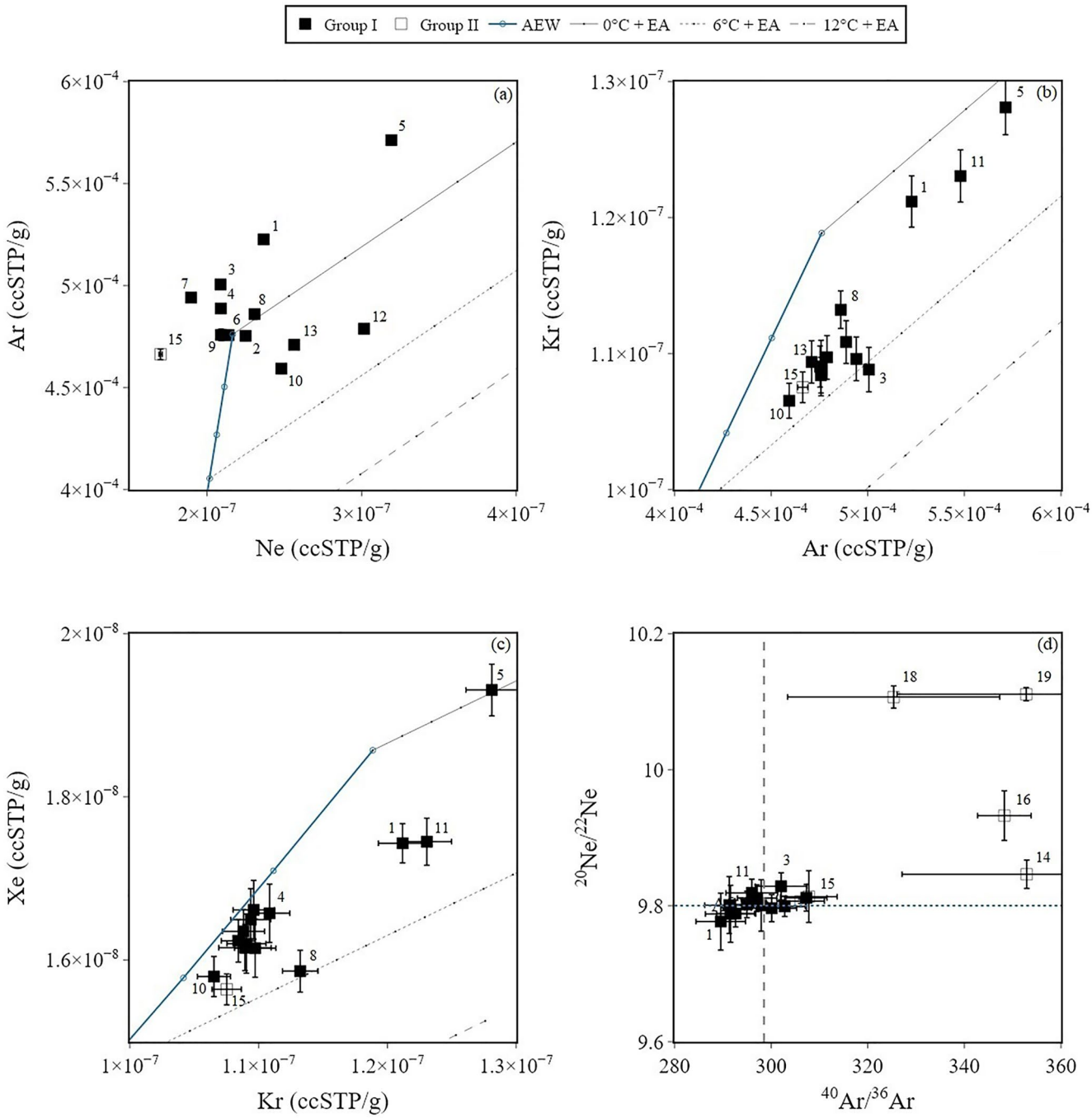

Figure 3. Measured Ar and Ne (a), Kr and Ar (b), Xe and Kr (c) plots compared to air-equilibrated water concentrations for 0–12°C and addition of unfractionated excess air and $^{20}Ne/^{22}Ne$ plotted against $^{40}Ar/^{36}Ar$ ratios and compared to the atmospheric $^{20}Ne/^{22}Ne$ (dashed black line) and $^{40}Ar/^{36}Ar$ (dotted blue line) ratio (d). Samples from group I are displayed as black squares, and samples from group II as open squares.

Contrary, based on the noble gas concentrations, $^{20}Ne/^{22}Ne$ and $^{40}Ar/^{36}Ar$ ratios, water chemistry, and stable water isotopes results, groundwater samples 1 to 13 from group I are not affected by Paleogene or Neogene groundwater or oil formation waters.

The $^{14}C_{DOC}$ and ^{81}Kr measurements from Winter and Einsiedl (2022) showed that samples from group I (1–5 and 11 to 13) are of Pleistocene/Holocene origin. We, therefore, assume that the noble gas record from these samples may be suitable for the determination of NGTs and reconstruction of the paleoclimate in Southern Germany during the Pleistocene.

Table 2
Fitting Results for Samples From Group I Using the Noble Gases Ar, Kr, and Xe and Ne, Ar, Kr, and Xe

		UA with Ar, Kr, and Xe						UA with Ne, Ar, Kr, and Xe					
			Prob. (%)	A	$A_{err.}$	NGT	$NGT_{err.}$		Prob. (%)	A	$A_{err.}$	NGT	$NGT_{err.}$
ID	Group	χ^2		cm^3STP/g		°C		χ^2		cm^3STP/g		°C	
1	I	1.29	25.67	8.39E−03	5.86E−04	2.45	0.39	169.39	0.00	1.03E−03	8.33E−05	−1.45	0.15
2		0.20	65.36	5.48E−03	6.44E−04	4.27	0.53	60.38	0.00	5.70E−04	3.32E−05	0.63	0.08
3		4.15	4.16	8.76E−03	5.57E−04	4.71	0.46	311.01	0.00	−6.68E−04	3.15E−05	−1.70	0.09
4		0.64	42.55	6.52E−03	6.46E−04	3.90	0.52	127.51	0.00	−5.80E−04	3.13E−05	−1.10	0.08
5		0.65	41.92	1.08E−02	6.38E−04	0.44	0.43	81.13	0.00	5.17E−03	4.58E−05	−2.93	0.09
6		1.46	22.65	5.75E−03	6.05E−04	4.45	0.42	91.30	0.00	1.46E−04	8.62E−05	1.23	0.17
7		2.15	14.28	7.53E−03	6.56E−04	4.29	0.54	217.60	0.00	−1.80E−03	2.88E−05	−2.17	0.07
8		3.68	5.50	6.76E−03	6.10E−04	4.31	0.42	95.31	0.00	1.08E−03	9.18E−05	1.12	0.17
9		0.19	66.24	5.47E−03	7.00E−04	4.19	0.50	69.17	0.00	−2.24E−04	7.57E−05	0.90	0.20
10		0.00	99.40	4.10E−03	5.77E−04	4.56	0.41	10.41	0.55	2.27E−03	9.77E−05	3.44	0.18
11		0.68	40.89	1.13E−02	6.02E−04	2.68	0.45	887.82	0.00	3.09E−02	1.02E−04	25.11	0.34
12		0.00	95.73	5.94E−03	6.53E−04	4.30	0.54	1.19	55.14	5.24E−03	4.30E−05	3.74	0.10
13		0.65	41.86	4.49E−03	6.63E−04	3.81	0.54	9.72	0.77	2.51E−03	3.72E−05	2.29	0.09

3.2. Fitting Procedure of the Noble Gas Record

Based on the data quality evaluation, we performed the fitting procedure described by Jung and Aeschbach (2018) for samples from group I. Interesting, we cannot find a best fit when we include Ne in the fitting procedure with the UA model and decided to exclude the measured Ne concentrations from further evaluation. As Ne is the least sensitive of the noble gases to the recharge temperature, it is characterized by the greatest diffusion coefficient of all measured noble gases and could potentially be affected by specific experimental issues; we decided to exclude the measured Ne concentrations from further evaluation. Restricting the fitting procedure to measured Ar, Kr, and Xe concentrations leads to good fits of the UA model for all samples of group I (Table 2). With only three data constraints for each sample, the simple UA model with two free parameters (T and A) is the sole option for the usual approach of PANGA to find the parameters that minimize the deviations of the model from the data in an overdetermined non-linear problem. Attempts to find solutions for models with three free parameters, such as the CE model with PANGA, did not yield sensible results for most samples (e.g., unphysical negative values for F). By prescribing values of the fractionation parameter F, the CE model can nonetheless be applied and yields good fits for F values up to 0.6, indicating at most moderate fractionation (note that $F = 0$ is equivalent to the UA model). However, the CE fits are not objectively preferable to the UA fits, and they yield very similar, though systematically slightly higher NGTs. Also, the good fits obtained with the CE model applied to all noble gases for samples 5, 10, 12, and 13 do not yield significantly different NGTs than the UA model fits, excluding Ne.

As a conclusion of the extensive data analysis and modeling efforts, we considered the results from fitting the noble gases Ar, Kr, and Xe with the UA model as most robust and appropriate for the interpretation and reconstruction of the paleoclimate (Table 2). For more detail of possible reasons for comparatively low Ne concentrations and that fits with PANGA using all measured noble gases fall short can be found in Supporting Information S1.

3.3. Reconstruction of the Late Pleistocene Climate in the SGMB

Calculation of the NGTs from the noble gas record in this way revealed NGTs between 0.4 (#5) and 4.7°C (#13) for samples 1–13. These NGTs indicate that most of the groundwater was recharged under cold climate conditions. Stable water isotopes further support this. Our samples show δ^2H values between −83.3 and −86.1‰ and $\delta^{18}O$ values between −10.7 and −11.8‰, which are typical of Pleistocene groundwater in this area (van Geldern et al., 2014) and further indicate groundwater recharge under cold climatic conditions. The calculated apparent $^{14}C_{DOC}$ groundwater ages for samples 1 to 5 and 11 to 13 range from approx. 10 to 26 ka. The apparent $^{14}C_{DOC}$

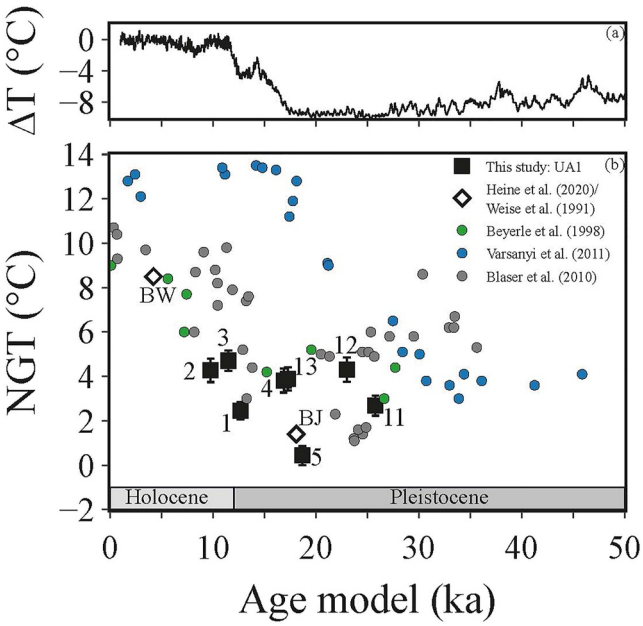

Figure 4. Illustration of a temperature model over the last 50 ka, derived from the EPICA Dome C ice core (Jouzel & Masson-Delmotte, 2007) in (a) and our $^{14}C_{DOC}$ model ages for samples 1 to 5 and 11 to 13 with NGTs combined with NGTs and $^{14}C_{DIC}$ ages model ages from other European studies in (b).

groundwater ages indicate that UJA groundwater may partially be recharged during the Late Pleistocene and early Holocene. The Pleistocene origin of parts of the UJA groundwater is further supported by apparent ^{81}Kr groundwater ages from the UJA, ranging between approx. 60 to 290 ka (Heidinger et al., 2019; Winter & Einsiedl, 2022).

For two other wells within the SGMB (BW and BJ), which are located in the western part of the study area and are also screened in the UJA, additional calculated NGTs and $^{14}C_{DOC}$ values are available from the literature, which were used for this study (Heine & Einsiedl, 2020; Weise et al., 1991). The apparent $^{14}C_{DOC}$ groundwater ages were calculated using the model described in Equation 3. The sample BW, which has an apparent groundwater age of 4 ka (Holocene), reflects a recharge temperature of 8.5°C. This correlates well with this region's modern long-term mean air temperature of 8–9°C (DWD, 2022). The sample BJ has an apparent groundwater age of 18 ka (Pleistocene) and is characterized by an NGT of 1.4°C. This result indicates that the mean temperature at the SGMB was around seven °C lower during the Pleistocene compared with modern times. Compared with the groundwater sample from location BW, all samples of this study clearly show colder NGTs between 0.4 (#5) and 4.7°C (#13) than the calculated 8.5°C of sample BW, which correlates well with the temperature rise between Late Pleistocene and Holocene derived from the EPICA Dome C ice core (Jouzel & Masson-Delmotte, 2007). Sample 5 shows even a colder NGT than sample BJ for the same period, at 0.4°C, which would lead to maximum cooling of approx. 8°C during the Pleistocene (Figure 4).

Samples 1, 2, and 3 are in the transition period between Pleistocene and Holocene. Their NGTs are still relatively cold, between 2.4 and 4.7°C, which is colder than expected from the temperature trend during this time (EPICA). For these three samples, Winter and Einsiedl (2022) assumed a mixing between a Pleistocene and Holocene groundwater component based on the stable water isotope signature and the finding of ^{81}Kr-ages for those samples. From the stable water isotope signature, the authors assumed a contribution of approx. 70% old, Pleistocene water, while 30% may stem from a young, Holocene component. This may explain the lower NGT during this time than expected from the temperature trend derived from locations BJ and BW.

The ΔT of the investigated groundwater samples, compared with the Holocene temperature of approx. 8.5°C estimated from location BW, varies between approx. 4 and 8°C. This correlates well with NGTs from other European studies (Figure 4), which found similar or slightly higher ΔT (Blaser et al., 2010; Varsányi et al., 2011) and is in excellent agreement with the global cooling of 6°C in low-to-mid-latitude land surfaces during the LGM (Seltzer et al., 2021).

In Figure 5a, from the δ^2H and δ^{18}O values and their relationship with the GMWL and LMWL, we can assume a meteoric origin of samples 1–13. Samples 3, 5, and 7 show an isotopic shift in the δ^{18}O values away from the LMWL toward a more enriched δ^{18}O signature, while other samples from group I do not show this isotopic shift in the δ^{18}O values. This is probably caused by more intense water-rock interaction, related to higher groundwater residence times for those samples, resulting in more enriched δ^{18}O values (Heine et al., 2021; Winter & Einsiedl, 2022). Generally, δ^{18}O contents of carbonate rocks are considerably higher than those of meteoric water and lead even by minor exchange processes (low water-rock ratio) and temperatures near 100°C to a more positive isotopic shift in δ^{18}O of water, as observed in our study.

Figure 5b displays the relationship between the stable water isotope δ^2H values and calculated NGTs. No clear relation between δ2H and NGTs is visible, as observed in other paleoclimate studies (Klump et al., 2008). All the samples from group I, except samples 1, 5, and 11, have NGTs around 4°C with corresponding δ^2H values between approx. −83 and −86‰. Samples 1, 5, and 11 show a higher variation in their NGTs between 0.4 and 2.7°C but the δ^2H values do not vary much with δ^2H values between −85.1 and −85.7‰. The stable water isotope signature reflects the mean annual air temperature (MAAT), while the NGT is related to the mean annual soil temperature (MAST). In general, the MAAT and MAST are related together. Therefore, we would expect

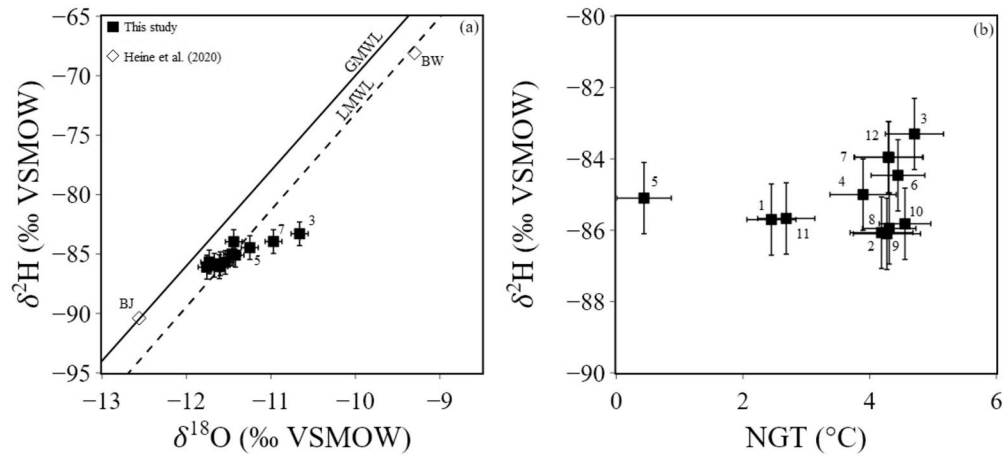

Figure 5. The differing relationship between δ^2H and $\delta^{18}O$ compared with GMWL (Craig, 1961) and LMWL (Stumpp et al., 2014) (a) and δ^2H and NGT (b) from sampled Upper Jurassic aquifer groundwater in the South German Molasse Basin.

lower δ^2H values with corresponding lower NGTs. But MAATs derived from weather stations can show significant deviations of up to 2°C from the MAST (Aeschbach-Hertig & Solomon, 2013). It is also stated in the literature that parameters, such as the thickness of snow cover on the soil, may influence heat transport and can produce either a warming or a cooling effect of ±1°C for the land surface (Aeschbach-Hertig & Solomon, 2013; Bartlett, 2004), shifting the MAST further away from the MAAT. In the UJA, the cover of the land surface with snow during the infiltration of the groundwater can cause a shielding effect, which was also observed, for example, by Blaser et al. (2010) in the Ledo-Paniselian Aquifer in Belgium. Similar to our results, this would also result in a decoupling between δ^2H values and NGTs.

Also, Ma et al. (2004) found a decoupling between $\delta^{18}O$ and NGT in Southern Michigan, which they related to a change in the atmospheric circulation pattern during the LGM. To test this hypothesis, the deuterium excess for the samples from group I, which do not show an isotopic shift in the $\delta^{18}O$ values due to intense water-rock interactions, was calculated and showed values lower than 6‰. These values are lower than the deuterium excess that was calculated from air masses coming either from the Atlantic (10‰) or the Mediterranean (up to 22‰) (Celle-Jeanton et al., 2001). And may not be a reasonable explanation for the observed decoupling process between δ^2H values and NGTs.

In modern times, the northern Alpine foreland air masses usually come from the Atlantic Ocean (van Geldern et al., 2014). However, Luetscher et al. (2015) proposed a change in the North Atlantic storm track during the LGM based upon $\delta^{18}O$ values from an Alpine speleothem record, resulting in a two to three times higher transportation of North Atlantic moisture from the South than today, with more depleted $\delta^{18}O$ values. This finding might indicate that Atlantic air masses from the South could recharge parts of the UJA groundwater.

Furthermore, the stable isotopic composition of groundwater samples 1–13 shows no evidence of UJA groundwater deriving from pure glacial meltwater as the $\delta^{18}O$ value of glacial meltwater of up to −25‰ is significantly lower than the measured $\delta^{18}O$ value of around −11.5‰ in groundwater (Klump et al., 2008). However, we cannot exclude that a mixture of glacial meltwater and meteoric water forms the UJA groundwater.

We assume a meteoric origin of the UJA groundwater from the stable water isotopes and groundwater infiltration in the glacial foreland during cold and dry periods based on the NGTs' results. The similar values of the analyzed parameters (NGTs, δ^2H, and $\delta^{18}O$, and hydrochemistry) for most of the samples from group I may be an additional indication that the UJA groundwater was recharged in an area with similar recharge conditions.

4. Conclusion

The results of this study indicate substantial soil cooling of up to 8°C in the SGMB during the Late Pleistocene compared with the Holocene temperature (8.5°C) after the LGM of the Alpine glaciers. Our observed NGTs in the SGMB agree well with other paleoclimate studies from other European aquifers, which found similar or

slightly higher temperature differences between the Holocene and Pleistocene. Based on the modeled NGTs, it can also be assumed that pronounced terrestrial cooling during the LGM was widespread through the interior European continent.

The evenly distributed NGT over the whole area of the SGMB may indicate similar recharge conditions for groundwater samples from group I in the UJA. The recharge conditions were under a cold climate, but no indications of pure glacial meltwater from δ^2H and $\delta^{18}O$ results were found. Groundwater recharge was probably driven mainly by meteoric water or a mixture of meteoric and glacial meltwater. The δ^2H and $\delta^{18}O$ signatures show typical values for Pleistocene groundwater but highlight the substantial differences between MAAT and MAST.

This study highlights the importance and usefulness of infiltration temperatures derived from the noble gas record in groundwater linked with the $^{14}C_{DOC}$ method for the reconstruction of the paleoclimate and investigation of recharge dynamics of the UJA in Southern Germany.

Our study may show for the first time that deep aquifer systems with groundwater circulation depths up to 5 km can contain Pleistocene groundwater with an atmospheric-derived noble gas composition, which can be used with careful interpretation and consideration of the hydrogeological setting to improve paleoclimate studies worldwide.

Data Availability Statement

The new noble gas, radiocarbon, and stable water isotope data used in this work arose from the projects IsoChem (Grant FKZ 104-0270-35385/2019) and GEOmaRe (Grant 0324331A). To compare our new data, we used already published data sets from Hungary (Varsányi et al., 2011), Belgium (Blaser et al., 2010), Switzerland (Beyerle et al., 1998) and the SGMB (Heine & Einsiedl, 2020; Weise et al., 1991; Winter & Einsiedl, 2022). The new data from this study was uploaded to the PANGAEA repository and is currently in the submission process. Temporarily, the data is uploaded in Supporting Information S1 for review purposes and will be accessible online in the PANGAEA repository upon acceptance of the article. The noble gas record was evaluated with the free program PANGA (v1.2) (Jung & Aeschbach, 2018). Figures were created with the Open-Source Graphing Library Plotly (v5.10.0) for Python, available at https://plotly.com/python/. Maps were created with the program ArcGIS Pro, requiring a license, by ESRI Inc. The software is available on the publisher's website at https://www.esri.com/de-de/arcgis/products/arcgis-pro/overview.

Acknowledgments
This work arose from the IsoChem (Grant FKZ 104-0270-35385/2019) project funded by the Bavarian State Ministry of Environment and Consumer Protection (StMUV). The authors want to thank all cooperating laboratories for their excellent and reliable cooperation, all owners of the geothermal energy plants sampled in this study for the opportunity to sample the groundwater and for enabling them to create the data basis for this study, and Stadtwerke München (SWM) for providing access to the newly constructed geothermal plant Schäftlarnstraße Munich within the framework of the associated GEOmaRe (Grant 0324331A) project funded through the Projektträger Jülich by the Federal Ministry for Economic Affairs and Climate Action. Special thanks goes to Thomas Fritzer from the Bavarian State Office for Environment and Geology for supporting the sampling of the three research wells. Finally, we want to thank two anonymous reviewers for their valuable comments, which helped to improve the manuscript. Open Access funding enabled and organized by Projekt DEAL.

References

Aeschbach-Hertig, W., El-Gamal, H., Wieser, M., & Palcsu, L. (2008). Modeling excess air and degassing in groundwater by equilibrium partitioning with a gas phase. *Water Resources Research*, *44*(8), 1–12. https://doi.org/10.1029/2007wr006454

Aeschbach-Hertig, W., Peeters, F., Beyerle, U., & Kipfer, R. (2000). Palaeotemperature reconstruction from noble gases in ground water taking into account equilibration with entrapped air. *Nature*, *405*(6790), 1040–1044. https://doi.org/10.1038/35016542

Aeschbach-Hertig, W., & Solomon, D. K. (2013). Noble gas thermometry in groundwater hydrology. In P. Burnard (Ed.), *The noble gases as geochemical tracers, advances in isotope geochemistry*. Springer-Verlag Berlin Heidelberg.

Aeschbach-Hertig, W., Stute, M., Clark, J. F., Reuter, R. F., & Schlosser, P. (2002). A paleotemperature record derived from dissolved noble gases in groundwater of the Aquia Aquifer (Maryland, USA). *Geochimica et Cosmochimica Acta*, *66*(5), 797–817. https://doi.org/10.1016/s0016-7037(01)00804-3

Andrews, J. N., & Lee, D. J. (1979). Inert gases in groundwater from the Bunter Sandstone of England as indicators of age and palaeoclimatic trends. *Journal of Hydrology*, *41*(3–4), 233–252. https://doi.org/10.1016/0022-1694(79)90064-7

Bartlett, M. G., Chapman, D. S., & Harris, R. N. (2004). Snow and the ground temperature record of climate change. *Journal of Geophysical Research*, *109*(F4), F04008. https://doi.org/10.1029/2004jf000224

Bertleff, B., Ellwanger, D., Szenkler, C., Eichinger, L., Trimborn, P., & Wolfendale, N. (1993). Interpretation of hydrochemical and hydroisotopical measurements on paleaogroundwaters in Oberschwaben, south German alpine foreland, with focus on quaternary geology. In *Proceedings of an international symposium on applications of isotope techniques in studying past and current environmental changes in the hydrosphere and the atmosphere*. Organized by the International Atomic Energy Agency. 19–23 April 1993, Bd. IAEA-SM-32.

Beyerle, U., Aeschbach-Hertig, W., Imboden, D. M., Baur, H., Graf, T., & Kipfer, R. (2000). A mass, spectrometric system for the analysis of noble gases and tritium from water samples. *Environmental Science and Technology*, *34*(10), 2042–2050. https://doi.org/10.1021/es990840h

Beyerle, U., Purtschert, R., Aeschbach-Hertig, W., Imboden, D. M., Loosli, H. H., Wieler, R., & Kipfer, R. (1998). Climate and groundwater recharge during the last glaciation in an ice-covered region. *Science*, *282*(5389), 731–734. https://doi.org/10.1126/science.282.5389.731

Blaser, P. C., Kipfer, R., Loosli, H. H., Walraevens, K., van Camp, M., & Aeschbach-Hertig, W. (2010). A 40 ka record of temperature and permafrost conditions in northwestern Europe from noble gases in the Ledo-Paniselian Aquifer (Belgium). *Journal of Quaternary Science*, *25*(6), 1038–1044. https://doi.org/10.1002/jqs.1391

Broers, H. P., Sültenfuß, J., Aeschbach, W., Kersting, A., Menkovich, A., Weert, J., & Castelijns, J. (2021). Paleoclimate signals and groundwater age distributions from 39 public water works in the Netherlands; Insights from noble gases and carbon, hydrogen and oxygen isotope tracers. *Water Resources Research*, *57*(7), e2020WR029058. https://doi.org/10.1029/2020wr029058

Celle-Jeanton, H., Travi, Y., & Blavoux, B. (2001). Isotopic typology of the precipitation in the Western Mediterranean Region at three different time scales. *Geophysical Research Letters*, *28*(7), 1215–1218. https://doi.org/10.1029/2000gl012407

Cey, B. D., Hudson, G. B., Moran, J. E., & Scanlon, B. R. (2009). Evaluation of noble gas recharge temperatures in a shallow unconfined aquifer. *Ground Water*, *47*(5), 646–659. https://doi.org/10.1111/j.1745-6584.2009.00562.x

Clark, I. (2015). Groundwater geochemistry and isotopes.

Clark, P. U., Dyke, A. S., Shakun, J. D., Carlson, A. E., Clark, J., Wohlfarth, B., et al. (2009). The Last Glacial Maximum. *Science*, *325*(5941), 710–714. https://doi.org/10.1126/science.1172873

Craig, H. (1961). Isotopic variations in meteoric waters. *Science*, *133*(3465), 1702–1703. https://doi.org/10.1126/science.133.3465.1702

Dansgaard, W. (1964). Stable isotopes in precipitation. *Tellus*, *16*(4), 436–468. https://doi.org/10.3402/tellusa.v16i4.8993

Dittmar, T., Koch, B., Hertkorn, N., & Kattner, G. (2008). A simple and efficient method for the solid-phase extraction of dissolved organic matter (SPE-DOM) from seawater. *Limnology and Oceanography: Methods*, *6*(6), 230–235. https://doi.org/10.4319/lom.2008.6.230

DWD. (2022). Climate Data Center (CDC)-Climate data for Germany.

Geyer, S., Wolf, M., Wassenaar, L., Fritz, P., Buckau, G., & Kim, J. (1993). Isotope investigations on fractions of dissolved organic carbon for ^{14}C groundwater dating.

Hayashi, M., Quinton, W. L., Pietroniro, A., & Gibson, J. J. (2004). Hydrologic functions of wetlands in a discontinuous permafrost basin indicated by isotopic and chemical signatures. *Journal of Hydrology*, *296*(1–4), 81–97. https://doi.org/10.1016/j.jhydrol.2004.03.020

Heidinger, M., Eichinger, F., Purtschert, R., Mueller, P., Zappala, J., Wirsing, G., et al. (2019). $^{81}Kr/^{85}Kr$-Dating of thermal groundwaters in the Upper Jurassic (Molasse Basin). *Grundwasser*, *24*(4), 287–294. https://doi.org/10.1007/s00767-019-00431-0

Heine, F., & Einsiedl, F. (2020). Applied geochemistry groundwater dating with dissolved organic radiocarbon: A promising approach in carbonate aquifers. *Applied Geochemistry*, *125*, 104827. https://doi.org/10.1016/j.apgeochem.2020.104827

Heine, F., Zosseder, K., & Einsiedl, F. (2021). Hydrochemical zoning and chemical evolution of the deep upper jurassic thermal groundwater reservoir using water chemical and environmental isotope data. *Water (Switzerland)*, *13*(9), 1162. https://doi.org/10.3390/w13091162

Hershey, R. L., Fereday, W., & Thomas, J. M. (2016). *Dissolved organic carbon ^{14}C in southern Nevada groundwater and implications for groundwater travel times* (Vol. 45268). Nevada University, Desert Research Institute. https://doi.org/10.2172/1287225

Jenkins, W. J., Lott, D. E., & Cahill, K. L. (2019). A determination of atmospheric helium, neon, argon, krypton, and xenon solubility concentrations in water and seawater. *Marine Chemistry*, *211*, 94–107. https://doi.org/10.1016/j.marchem.2019.03.007

Jouzel, J., & Masson-Delmotte, V. (2007). EPICA Dome C Ice Core 800KYr deuterium data and temperature estimates. Supplement to: Jouzel, Jean; Masson-Delmotte, Valerie; Cattani, Olivier; Dreyfus, Gabrielle; Falourd, Sonia; Hoffmann, G; Minster, Bénédicte; Nouet, Julius; Barnola, Jean-Marc; Chappellaz, Jérôme A; Fischer, Hubertus; Gallet, J C; Johnsen, Sigfús Jóhann; Leuenberger, Markus Christian; Loulergue, Laetitia; Luethi, D; Oerter, Hans; Parrenin, Frédéric; Raisbeck, Grant M; Raynaud, Dominique; Schilt, Adrian; Schwander, Jakob; Selmo, Enricomaria; Souchez, Roland A; Spahni, Renato; Stauffer, Bernhard; Steffensen, Jørgen Peder; Stenni, Barbara; Stocker, Thomas F; Tison, Jean-Louis; Werner, Martin; Wolff, Eric William (2007): Orbital and millennial Antarctic climate variability over the past 800,000 years. *Science*, *317*(5839), 793–797. https://doi.org/10.1126/science.1141038

Jung, M., & Aeschbach, W. (2018). A new software tool for the analysis of noble gas data sets from (ground)water. *Environmental Modelling and Software*, *103*, 120–130. https://doi.org/10.1016/j.envsoft.2018.02.004

Karolytė, R., Barry, P. H., Hunt, A. G., Kulongoski, J. T., Tyne, R. L., Davis, T. A., et al. (2021). Noble gas signatures constrain oil-field water as the carrier phase of hydrocarbons occurring in shallow aquifers in the San Joaquin Basin, USA. *Chemical Geology*, *584*, 120491. https://doi.org/10.1016/j.chemgeo.2021.120491

Klump, S., Grundl, T., Purtschert, R., & Kipfer, R. (2008). Groundwater and climate dynamics derived from noble gas, ^{14}C, and stable isotope data. *Geology*, *36*(5), 395. https://doi.org/10.1130/g24604a.1

Lee, J. Y., Marti, K., Severinghaus, J. P., Kawamura, K., Yoo, H. S., Lee, J. B., & Kim, J. S. (2006). A redetermination of the isotopic abundances of atmospheric Ar. *Geochimica et Cosmochimica Acta*, *70*(17), 4507–4512. https://doi.org/10.1016/j.gca.2006.06.1563

Li, Y., Harir, M., Lucio, M., Kanawati, B., Smirnov, K., Flerus, R., et al. (2016). Proposed guidelines for solid phase extraction of Suwannee River dissolved organic matter. *Analytical Chemistry*, *88*(13), 6680–6688. https://doi.org/10.1021/acs.analchem.5b04501

Luetscher, M., Boch, R., Sodemann, H., Spötl, C., Cheng, H., Edwards, R. L., et al. (2015). North Atlantic storm track changes during the Last Glacial Maximum recorded by Alpine speleothems. *Nature Communications*, *6*(1), 6344. https://doi.org/10.1038/ncomms7344

Ma, L., Castro, M. C., & Hall, C. M. (2004). A late Pleistocene–Holocene noble gas paleotemperature record in southern Michigan. *Geophysical Research Letters*, *31*(23), L23204. https://doi.org/10.1029/2004gl021766

McIntosh, J. C., Schlegel, M. E., & Person, M. (2012). Glacial impacts on hydrologic processes in sedimentary basins: Evidence from natural tracer studies. *Geofluids*, *12*(1), 7–21. https://doi.org/10.1111/j.1468-8123.2011.00344.x

Murphy, E. M., Davis, S. N., Long, A., Donahue, D., & Jull, A. T. (1989). Characterization and isotopic composition of organic and inorganic carbon in the Milk River Aquifer. *Water Resources Research*, *25*(8), 1893–1905. https://doi.org/10.1029/WR025i008p01893

Nakata, K., Hasegawa, T., Solomon, D. K., Miyakawa, K., Tomioka, Y., Ohta, T., et al. (2019). Degassing behavior of noble gases from groundwater during groundwater sampling. *Applied Geochemistry*, *104*, 60–70. https://doi.org/10.1016/j.apgeochem.2019.03.007

Pepin, R. O., & Porcelli, D. (2002). Origin of noble gases in the terrestrial planets. *Reviews in Mineralogy and Geochemistry*, *47*(1), 191–246. https://doi.org/10.2138/rmg.2002.47.7

Porcelli, D., Ballentine, C. J., & Wieler, R. (2002). An overview of noble gas geochemistry and cosmochemistry. *Reviews in Mineralogy and Geochemistry*, *47*(1), 1–19. https://doi.org/10.2138/rmg.2002.47.1

Seltzer, A. M., Ng, J., Aeschbach, W., Kipfer, R., Kulongoski, J. T., Severinghaus, J. P., & Stute, M. (2021). Widespread six degrees Celsius cooling on land during the Last Glacial Maximum. *Nature*, *593*(7858), 228–232. https://doi.org/10.1038/s41586-021-03467-6

Stichler, W. (1997). Isotopengehalte in Tiefengrundwässern aus Erdöl-und Erdgasbohrungen im süddeutschen Molassebecken. *Beiträge zur Hydrogeologie*, *48*, 81–88.

Stumpp, C., Klaus, J., & Stichler, W. (2014). Analysis of long-term stable isotopic composition in German precipitation. *Journal of Hydrology*, *517*, 351–361. https://doi.org/10.1016/j.jhydrol.2014.05.034

Stute, M., Forster, M., Frischkorn, H., Serejo, A., Clark, J. F., Schlosser, P., et al. (1995). Cooling of tropical Brazil (5°C) during the Last Glacial Maximum. *Science*, *269*(5222), 379–383. https://doi.org/10.1126/science.269.5222.379

Stute, M., & Schlosser, P. (1993). Principles and applications of the noble gas paleothermometer. In P. K. Swart, K. C. Lohmann, J. McKenzie, & S. Savin (Eds.), *Climate Change in Continental Isotopic Records*. American Geophysical Union.

Thomas, J. M., Hershey, R. L., Fereday, W., & Burr, G. (2021). Using Carbon-14 of dissolved organic carbon to determine groundwater ages and travel times in aquifers with low organic carbon. *Applied Geochemistry*, *124*, 104842. https://doi.org/10.1016/j.apgeochem.2020.104842

Utting, N., Lauriol, B., Mochnacz, N., Aeschbach-Hertig, W., & Clark, I. (2013). Noble gas and isotope geochemistry in western Canadian Arctic watersheds: Tracing groundwater recharge in permafrost terrain. *Hydrogeology Journal*, *21*(1), 79–91. https://doi.org/10.1007/s10040-012-0913-8

van Geldern, R., Baier, A., Subert, H. L., Kowol, S., Balk, L., & Barth, J. A. C. (2014). Pleistocene paleo-groundwater as a pristine fresh water resource in southern Germany--Evidence from stable and radiogenic isotopes. *Science of the Total Environment*, *496*, 107–115. https://doi.org/10.1016/j.scitotenv.2014.07.011

Varsányi, I., Palcsu, L., & Kovács, L. Ó. (2011). Groundwater flow system as an archive of palaeotemperature: Noble gas, radiocarbon, stable isotope and geochemical study in the Pannonian Basin, Hungary. *Applied Geochemistry*, *26*(1), 91–104. https://doi.org/10.1016/j.apgeochem.2010.11.006

Weise, S., Wolf, M., Fritz, P., Rauert, W., Stichler, W., Prestel, R., et al. (1991). Isotopenhydrologische Untersuchungen im Süddeutschen Molassebecken. In Bayer. LfW & LGRB (Eds.), [Hrsg.], *Hydrogeothermische Energiebilanz und Grundwasserhaushalt des Malmkarstes im süddeutschen Molassebecken. – Schlussbericht zum Forschungsvorhaben 03E–6240 A/B (im Auftrag des Bundesministeri-ums für Forschung und Technologi)*.

Weyhenmeyer, C. E., Burns, S. J., Waber, H. N., Aeschbach-Hertig, W., Kipfer, R., Loosli, H. H., & Matter, A. (2000). Cool glacial temperatures and changes in moisture source recorded in Oman groundwaters. *Science*, *287*(5454), 842–845. https://doi.org/10.1126/science.287.5454.842

Winter, T., & Einsiedl, F. (2022). Combining ^{14}CDOC and ^{81}Kr with hydrochemical data to identify recharge processes in the South German Molasse Basin. *Journal of Hydrology*, *612*, 128020. https://doi.org/10.1016/j.jhydrol.2022.128020